ACS APPLIED MATERIALS & INTERFACES

Research Article

www.acsami.org

Impact of Nanostructure on Mechanical Properties of Norbornene-based Block Copolymers under Simulated Operating Conditions for Biobutanol Membranes

Changhuai Ye,[†] Tamami Takigawa,[‡] Oleksandr (Sasha) Burtovyy,[‡] Leah Langsdorf,[‡] Dane Jablonski,[‡] Andrew Bell,[‡] and Bryan D. Vogt*[,†]

[†]Department of Polymer Engineering, University of Akron, Akron, Ohio 44325, United States

[‡]Promerus, LLC, 9921 Brecksville Road, Brecksville, Ohio 44107, United States

Supporting Information

ABSTRACT: The structure and mechanical properties of a novel block copolymer (BCP) system with T_g's for both segments exceeding 300 °C, poly(butylnorbornene)-*block*-poly(hydroxyhexafluoroisopropyl norbornene) (BuNB-*b*-HFANB), are investigated as a function of processing conditions used for solvent vapor annealing (SVA). Solvent selection impacts long-range order markedly, but unexpectedly vertical orientation of cylinders are preferred over a wide range of solubility parameters, as determined by atomic force microscopy and grazing incidence small-angle X-ray scattering. The mechanical properties (elastic modulus, fracture strength, and onset fracture strain) are dependent upon the long-range order induced during SVA and determined using the combination of surface wrinkling and cracking. The modulus and fracture strength of the films increase from 1.44 GPa and 12.1 MPa to 1.77 GPa and 17.5 MPa, respectively, whereas the onset fracture strain decreases from 1.6% to approximately 0.6% as the ordering is improved. The polarity difference in the segments of the BCP is attractive for membrane separations, especially butanol−water. For biobutanol recovery, the titers are typically <3 wt % butanol; exposure of the BCP membrane to aqueous 1 wt % butanol decreases the elastic modulus to approximately 0.90 GPa, irrespective of the morphology, despite the high T_g of both segments and limited swelling (5.0 wt %). Correspondingly, the onset fracture strain of these swollen films is estimated to increase significantly to 6−7%. These results indicate that operating conditions impact the mechanical performance of BCP membranes more than their morphology despite the high T_g of the neat copolymer. Wrinkling and cracking provide a facile route to test the mechanical properties of membranes under simulated operando conditions.

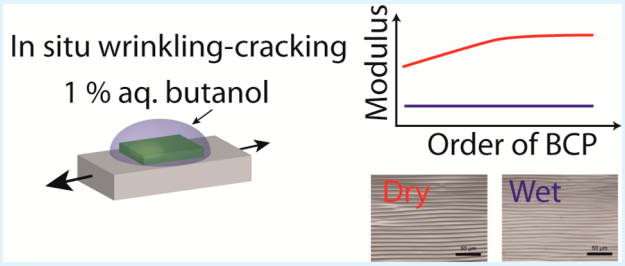

KEYWORDS: *QCM-D, wrinkling, cracking, Young's modulus, ABE separations*

INTRODUCTION

Block copolymers (BCPs) provide a facile route to nanostructured materials with orthogonal or complementary properties that cannot be easily obtained in a single material.[1] For example, the combination of glassy and rubbery segments of BCPs provides the basis for easily processable thermoplastic elastomers.[2] In these BCPs, the mechanical properties are the critical properties for their commercialization as elastomers; typical polymer processing induces orientation of the self-assembled nanostructure, which leads to significant enhancements in the mechanical properties in bulk BCPs.[3] Alternatively, BCPs have been considered as potential advanced materials in separations as membranes, where the matrix component generally acts to provide durability, while the minority component facilitates selective transport across the membrane.[4] In these cases, the morphology and alignment typically impact the performance of the membrane in terms of flux and selectivity.[5,6] One major advantage of membrane separations is its inherently low energy operation in comparison to other traditional separation processes, such as distillation;[7] this is particularly important for generation of green fuels where the energy consumption associated with separations can be a significant fraction of the gross energy density obtained from the fuel.[8] In comparison to ethanol, biobutanol can be more directly substituted for gasoline.[9] Butanol also offers advantages associated with its larger energy density and limited water solubility as a liquid fuel over ethanol. Two challenges that are hindering the development of butanol as a next generation biofuel are (i) limited concentration of butanol in the fermentation broth due to toxicity that limits increasing titer concentration and (ii) high distillation costs associated with water removal.[10] BCP membranes potentially offer advantages associated with decoupling of the transport and mechanical integrity by selection of segments.[11] Recently, Balsara and co-workers examined the role of morphology through variation in the volume fraction on the performance of polystyrene-*block*-

Received: December 21, 2014
Accepted: May 18, 2015
Published: May 18, 2015

DOI: 10.1021/acsami.5b02692
ACS Appl. Mater. Interfaces 2015, 7, 11765−11774

polybutadiene-*block*-polystyrene for ethanol separations.[6] The morphology of the BCP membrane will couple with the separation efficiency, as has been examined previously, but will also impact the mechanical integrity of the membrane. For transport through a BCP membrane, the vertical orientation of cylindrical domains is generally assumed desired if the minority phase is primarily responsible for permeation, but there are significant hurdles involved in achieving this orientation.

The interfaces of the BCP with air and the substrate support produce forces that tend to produce parallel alignment of anisotropic morphologies (cylinders and lamellae) with respect to the interfaces.[12] In the past, there have been tremendous efforts to overcome these interactions in BCPs to produce vertically alignment morphologies[13] for microelectronics applications,[14] in particular for directed self-assembly.[15] The modification of substrate to provide neutral wetting conditions[16] or selective wetting from lithographic patterning[17] has been effective for the vertical alignment in poly(styrene-*block*-methyl methacrylate). Similarly, Willson and co-workers have recently demonstrated the use of a top-coat to mitigate free surface wetting.[18,19] These methods are typically limited, however, for alignment of BCP domains through thicknesses commonly encountered in membranes (1−10 μm). Electric fields[20,21] and thermal gradients[22] have been shown to align thicker films (ca. 1 μm), but the efficacy of these processes will be dependent on the physicochemical properties of the blocks. Interestingly, for thin BCP films, the vertical alignment of cylindrical domains can occur spontaneously during spin coating with the use of the correct solvent for casting.[23] As solvent−polymer interactions can impact the interfacial properties, solvent can be utilized to control the orientation in BCP films through solvent vapor annealing (SVA).[24] The exposure of the BCP film to solvent vapors induces plasticization of the film to provide mobility for segmental reorganization, which tends to enhance also the long-range order in the BCP films.[25] By tuning the selectivity of the solvent used in SVA, the orientation of cylindrical morphology in BCPs can be varied from parallel to vertical.[26,27] The variation in solvent properties by use of mixtures provides a facile route to tuning the morphology of BCP films using SVA.[27,28] These processing steps are necessary in most cases, as the non-neutral wetting conditions for most BCP films with anisotropic morphologies tend to favor the parallel orientation.

Although high permselectivity of the BCP membrane is necessary for commercialization, it is not a sufficient characteristic alone. The durability of the membrane (mechanical integrity) is also a critical factor as the membrane is exposed to a pressure drop during operation and assembly. The mechanical measurements of such thin polymer coatings is challenging and thus insight into failures that occur during membrane operation have generally been limited to modeling.[29] Very recently, the mechanical properties of polyamide membranes have been examined in the thin film morphology.[30] These measurements have been enabled by the establishment of new metrologies based on wrinkling[31] and cracking[30] of the membranes attached to soft elastomeric substrates. Much is known about the mechanical properties of bulk thermoplastic elastomers based on BCPs,[3,32,33] but the mechanical properties of BCP thin films and membranes[34] are much less examined. Crosby and co-workers have illustrated that the nanoscale morphology of the BCP impacts crazing behavior[35] and surface topology resulting from islands and holes produces stress localization.[36] These results indicate that the morphology of the BCP membrane may dramatically impact the mechanical properties, but the influence of morphology on the mechanical properties, especially under conditions associated with operation, is not known.

In this paper, we examine how nanostructure influences the mechanical properties of a novel diblock copolymer membrane. The BCP is synthesized by addition polymerization of butyl norbornene and hydroxyhexafluoroisopropyl norbornene (BuNB-*b*-HFANB), which yields a bicyclic ring in each repeat unit that leads to a rigid backbone and high glass transition temperature (T_g > 300 °C). This BCP offers polarity contrast for potential separation of biobutanol with HFANB envisioned as the transport phase for the butanol, whereas BuNB offers mechanical reinforcement for the membrane and hydrophobicity to minimize the water flux. Here, the morphology is modulated using SVA and the morphology is correlated to their mechanical properties using wrinkling and cracking. We seek to answer the following questions: (1) Are mechanical properties of these BCP membranes sensitive to minor changes in the ordering of the system? and (2) How are these properties impacted by exposure to conditions that mimic operation as a biobutanol membrane? Herein, we demonstrate that wrinkling-cracking measurements provide insight into the mechanical properties of polymer membranes during operation and can sense subtle changes in the processing dependent morphology of BCP membranes.

EXPERIMENTAL SECTION

Materials. 1-Butanol (>99%, ACS reagent), toluene (>99.5%, ACS reagent), tetrahydrofuran (THF, >99.0%, ACS reagent with 250 ppm BHT), 1,4-dioxane (>99.0%, ACS reagent), and dimethylformamide (DMF, >99.8%, ACS reagent) were obtained from Sigma-Aldrich and used as received. The block copolymer was synthesized sequentially starting with high purity BuNB monomer and then HFANB monomers are added after the BuNB has been consumed using a proprietary (trialkylphosphine) Pd-based initiator.[37] The HFANB monomer was selected, as it generates an alcohol soluble polymer that is not soluble in neutral water to provide a selective transport phase. The BCP was purified by standard techniques to remove any catalyst residues and residual monomer.

The molecular weight of BuNB-*b*-HFANB was characterized by gel permeation chromatography (GPC). THF was used as eluent. The measurement was carried out at a flow rate of 1 mL/min at 40 °C using an RI detector. On the basis of the GPC data (Figure S1 of the Supporting Information) using polystyrene standards, the number-average molecular weight (M_n) and the polydispersity index of BuNB-*b*-HFANB were 106 kg/mol and 1.18, respectively. The molar ratio of BuNB to HFANB in BuNB-*b*-HFANB was 0.55:0.45 as determined from ^{13}C NMR (Figure S2 of the Supporting Information). The densities of the respective homopolymers were measured using a gas pycnometer with helium (Micromeritics Instrument Corporation Accupyc II 1340). The density of BuNB homopolymer is 0.96 g/cm^3 whereas the density of HFANB homopolymer is 1.42 g/cm^3, which is consistent with its previously reported density.[38] Thus, the volume fraction of HFANB (f_{HFA}) is approximately 0.5. The glass transition temperatures of the individual components are approximately 340 and 360 °C for BuNB and HFANB, respectively.

Film Preparation and Processing. Silicon wafers (University Wafer, resistivity: 3−50 ohm·cm), which were cleaved into approximately 1.5 cm × 1.5 cm pieces, were used as substrates. Prior to spin coating, the substrates were cleaned by piranha solution (7:3 H_2SO_4:30 wt % H_2O_2) at 90 °C for 30 min, then subsequently rinsed with deionized water several times to generate a clean hydroxylated surface. ***Caution***: *piranha solution is aggressive and explosive. Never mix piranha waste with solvents. Check the safety precautions before using it.* For QCM-D measurements, gold quartz crystals (QSX301, Biolin Scientific, Inc.) were used as substrates and

DOI: 10.1021/acsami.5b02692
ACS Appl. Mater. Interfaces 2015, 7, 11765−11774

cleaned with ultraviolet ozone (UVO, PSD series Digital UV Ozone System, Novascan Technologies, Inc.) for 30 min before spin coating. Films were prepared by spin coating from 3.5 wt % BuNB-*b*-HFANB toluene solution at 2500 rpm onto the silicon wafers or quartz sensors. The thicknesses of the films were typically between 140 and 150 nm.

A flow system using two mass flow controllers (MKS-146C-FF000-1) was utilized for controlling the atmosphere around the film for the SVA process; this setup was similar to those of other reports.[27,28] One gas stream was dry air, whereas the other stream was nearly saturated solvent vapor, generated by bubbling dry air through the liquid solvent. Four different solvents were utilized for SVA: toluene, THF, 1,4-dioxane, and DMF. For these SVA studies, the films were exposed to nearly saturated solvent vapor at 800 mL/min at ambient temperature for 3 h; the films were then dried at 40 mL/min for approximately 12 h with dry air. Subsequently, the films were heated at 50 °C *in vacuo* for approximately 12 h to remove any residual solvent.

Characterization. The thickness and refractive index of the films were measured with a variable angle spectroscopic ellipsometer (VASE, J.A. Woollam Co., Inc.). Measurements were performed from 60° to 75° in 5° increments using wavelengths from 246 to 1689 nm. The ellipsometric data were fit using the Cauchy dispersion to describe the optical properties of the BuNB-*b*-HFANB film. The swelling dynamics and uptake during SVA with the different solvents was elucidated from *in situ* ellipsometry measurements using a sealed cell with quartz windows fixed at 70°. Details about the cell are provided in the Supporting Information of reference 39.

The solvent uptake into the BuNB-*b*-HFANB films from aqueous butanol solutions was determined using QCM-D (Q-Sense, Flow module 401)[40] with a flow rate of 0.1 mL/min at 37 °C. To separate the effects of absorption in the film and the change in viscosity associated with the addition of butanol to water, baseline measurements were performed using the solutions of interest with an uncoated quartz sensor. The same solution concentrations were then utilized when the sensor was coated with a nominally 150 nm thick BuNB-*b*-HFANB film. By examining the difference in both frequency and dissipation shift associated with the aqueous butanol solutions with and without the BuNB-*b*-HFANB, the effective sorption into the BCP film was determined. Because of the glassy nature of the BCP, the dissipation changes observed were almost solely attributable to the viscosity of the solution.[41] Thus, the mass uptake into the BuNB-*b*-HFANB was calculated using the Sauerbrey expression.[42]

The surface morphology of the films was characterized by atomic force microscopy (AFM, Dimension V, Veeco Instruments Inc.) operating in tapping mode using silicon tips (ACT-100, Applied Nanostructures, Inc.). A constant scan size of 2 μm × 2 μm at 1 Hz was used for all measurements. The nanostructure of the BCP films was further investigated by grazing incidence small-angle X-ray scattering (GISAXS) using an incident X-ray energy of 13.5 keV at the X9 beamline at the National Synchrotron Light Source (NSLS) at Brookhaven National Laboratory. The scattered photons were measured with a charged-coupled device (CCD) detector at 5 m (sample-to-detector distance). The incident angle was varied from 0.07° to 0.25° in order to transverse through the critical angle of the film to enable examination of both the surface and bulk structure. Because of the low X-ray contrast between BuNB and HFANB, the exposure time for each measurement with GISAXS was 30 s.

Transmission electron microscopy (TEM) was used to characterize further the microphase separated structure of BuNB-*b*-HFANB films. The BuNB-*b*-HFANB films were floated on water from silicon wafer and collected by TEM grids (300 mesh Cu, TED PELLA Inc.). To increase the electron contrast between BuNB and HFANB domains, the samples were stained using RuO_4 vapor for 1 h. To identify which phase is the majority phase in microphase separated BuNB-*b*-HFANB films, cross-sectional TEM was performed for a bilayer BuNB/HFANB homopolymers that consists of approximately 400 nm thick FHANB layer spun coated from ethanol on top of a 150 nm thick BuNB homopolymer. This bilayer film was coated with Ag on the surface for 2 min with a K575 sputter coater. To perform cross-sectional TEM on this sample, the film was first floated on the water and then embedded in epoxy resin, cured and sectioned using microtome. The sample was stained using RuO_4 with the same condition as that for BuNB-*b*-HFANB film before TEM.

Mechanical Measurements. The elastic modulus of the BuNB-*b*-HFANB films was measured using surface wrinkling.[31] Poly(dimethylsiloxane) (PDMS, Sylgard 184, Dow Corning) was used as the compliant substrate for these measurements and prepared with a mass ratio of base to curing agent of 20:1. The well-mixed base and curing agent was cast on a flat glass plate and precured/degassed at the ambient temperature for 4 h. Then, the PDMS was further cured at 120 °C for 3 h. The elastomer was cut into 2.5 cm × 7.5 cm strips after cooling to ambient temperature to generate the substrate for wrinkling. The elastic modulus of the PDMS was determined using a Texture analyzer (TA-TX Plus, Stable Micro Systems) at a strain rate of 0.05 mm/s. To generate the wrinkles, the PDMS slabs were prestrained to 3.5−4.0% using a custom strain stage[43] and films of BuNB-*b*-HFANB film were transferred to PDMS from silicon substrates by differential adhesion in water. After transfer, the polymer thin films were dried at ambient conditions for 12 h. The wrinkling was induced by release of the prestrain at a rate of 0.1 mm/s using a Universal Motion Controller (Model: Esp100, Newport Corporation). For the elastic modulus measurement of swollen films with butanol, aqueous 1% butanol solution was dropped on the surface to cover completely the transferred films on PDMS. After waiting 20 min for the solution to equilibrate, the prestrain was released to induce the surface wrinkling. To investigate the swelling of the PDMS substrate by aqueous 1 wt % butanol solution, the thickness change of a thin layer of PDMS coated on silicon wafer before and after immersing in aqueous 1 wt % butanol solution was characterized using VASE. The thickness change for PDMS after 20 min of immersion was less than 1 nm for the PDMS film with a dry thickness of 870 nm. Thus, the PDMS substrate is not impacted by the 1 wt % butanol solution. The surface wrinkles of the BCP films were quantified using an optical microscopy (Olympus MX51, Olympus Corporation). The wavelength of the wrinkling was elucidated from these optical micrographs using a fast Fourier transform (FFT). For each sample, a minimum of 7 images was utilized to calculate the wrinkling wavelength, λ. At the low strains (3.5−4%) utilized, the PDMS is linear elastic, which combined with the large difference in thickness between the PDMS and film provides a simple relationship for the modulus of the film, $\overline{E}_f$:[31,43]

$$\overline{E}_f = 3\overline{E}_s\left(\frac{\lambda}{2\pi h}\right)^3$$

where $\overline{E}_s$ is the plane-strain modulus of the PDMS substrate and h is the film thickness.

Cracking measurements were conducted on the same custom strain stage as wrinkling measurement using the Universal Motion Controller to control each step of stretching strain. The PDMS substrate (base:curing agent = 15:1) was loaded onto the strain stage without any prestrain. The thin films were then transferred to PDMS by the same water immersion technique and dried at ambient condition for 12 h. Subsequently, the PDMS substrate was stretched to 1−2% strain at a strain rate of 0.1% strain per second until a few cracks were observed on the thin films by optical microscopy. Then the substrate was stretched in 0.3% strain steps and images of the cracks at each step were recorded using an optical microscope (Olympus MX51, Olympus Corporation). The crack spacing was calculated from the cracks over an area of approximately 9.2 mm × 7.0 mm. The fracture strength and the onset fracture strain of each sample were derived using at least 3 films. The onset fracture strain of films immersed in 1 wt % aqueous butanol was estimated by observing the first appearance of cracks in the thin films while increasing the stretching strain in 1% steps.

RESULTS AND DISCUSSION

For SVA to order effectively the BCP, the BCP film must be sufficiently swollen by the solvent(s) to enable sufficient plasticization for chain rearrangements. Figure S3 in the Supporting Information illustrates the sorption isotherms of the four solvents for the BuNB-*b*-HFANB films. Interestingly,

DOI: 10.1021/acsami.5b02692
ACS Appl. Mater. Interfaces 2015, 7, 11765−11774

the quasi-equilibrium swelling is nearly invariant of solvent selection with approximately 23 vol % swelling for toluene, 21 vol % for THF, and 26 vol % for dioxane; there is a modest increase in the swelling for the most polar solvent, DMF, to nearly 36%, but this difference in solubility in the BCP is not as significant as typically observed for such a broad range of solvents.[44] The aliphatic (BuNB) and polar (NFANB) side groups on the norbornene backbone provides a large difference in Hildebrand solubility parameters, δ, for each block, as calculated by group contribution (see the Supporting Information for details on these calculations), as shown in Table 1. These solubility parameters should result in significant differences in the relative solubility in the different segments. The swelling of the BuNB and HFANB homopolymers (see Figure S4 in the Supporting Information) demonstrates that the solvents are selective for HFANB segments except toluene, which appears to be slightly selective to the BuNB. The differences in the quasiequilibrium swelling of BuNB-*b*-HFANB films are relatively small, so the effect of solvent selection during SVA on the morphology and other properties should be primarily related to the solvent selectivity and specific interactions of the solvents with the BCP segments, not simply due to differences in solubility (extent of plasticization).

Table 1. Hansen Solubility Parameters[45] Associated with Solvents and Each Segment of BuNB-*b*-HFANB[a]

	δ_d (MPa)$^{1/2}$	δ_p (MPa)$^{1/2}$	δ_h (MPa)$^{1/2}$	δ (MPa)$^{1/2}$
HFANB[b]	13.8	17.4	10.3	24.5
BuNB[b]	14.0	0	0	14.0
dioxane	19.0	1.8	7.4	20.5
DMF	17.4	13.7	11.3	24.9
THF	16.8	5.7	8.0	19.5
toluene	18.0	1.4	2.0	18.2

[a]δ_d is energy associated with dispersive forces, δ_p is energy associated with dipole forces, and δ_h is energy associated with hydrogen bonding. [b]Values calculated by group contribution methods.

The high T_g associated with the BuNB-*b*-HFANB prevents formation of a highly ordered morphology by thermal annealing (annealing at 220 °C for 42 h results in no change and further increases in temperature result in some degradation) without degradation of the BCP (Figure S5 of the Supporting Information). Figure 1 illustrates the efficacy of SVA in ordering the BuNB-*b*-HFANB film as determined by the surface morphology from AFM. One intriguing note about this BuNB-*b*-HFANB is that the composition is symmetric on a volumetric basis, so lamellae are expected but a cylindrical morphology is always observed. The selectivity of the casting solvent is known to impact the morphology of block copolymer films, which may shift the morphology.[46] However, the BuNB-*b*-HFANB films are cast initially from toluene (slightly selective to BuNB) and cylinders are observed from the as-cast to any SVA condition used that are selective to HFABN, except toluene. The HFANB comprises the majority phase, as determined from TEM (Figure S6 of the Supporting Information). For the film annealed using toluene (Figure 1A), the surface morphology is composed of short lines and circles (either spheres or vertical cylinders) with little ordering at the size scale consistent with self-assembly; this is a slight improvement in the ordering of the film prior to SVA where the surface shows limited nanoscale structures and no clear sign of ordering (Figure 1E), as evidenced by the FFT shown in the inset. The domains become better defined, but the ordering of these nanostructures is extremely limited. The ordering is likely kinetically limited by the mobility of the BCP segments.

One possible explanation for this poor ordering is due to the hydrogen bonding cooperativity associated with hydroxyl groups in HFANB, which cannot be readily exchanged with toluene because toluene has a small hydrogen-bonding basicity (β^H) of ~0.14.[47] To examine this influence, THF (β^H = 0.48), dioxane (β^H = 0.64), and DMF (β^H = 0.74) are examined as the hydrogen bond acceptor strength increases systematically for

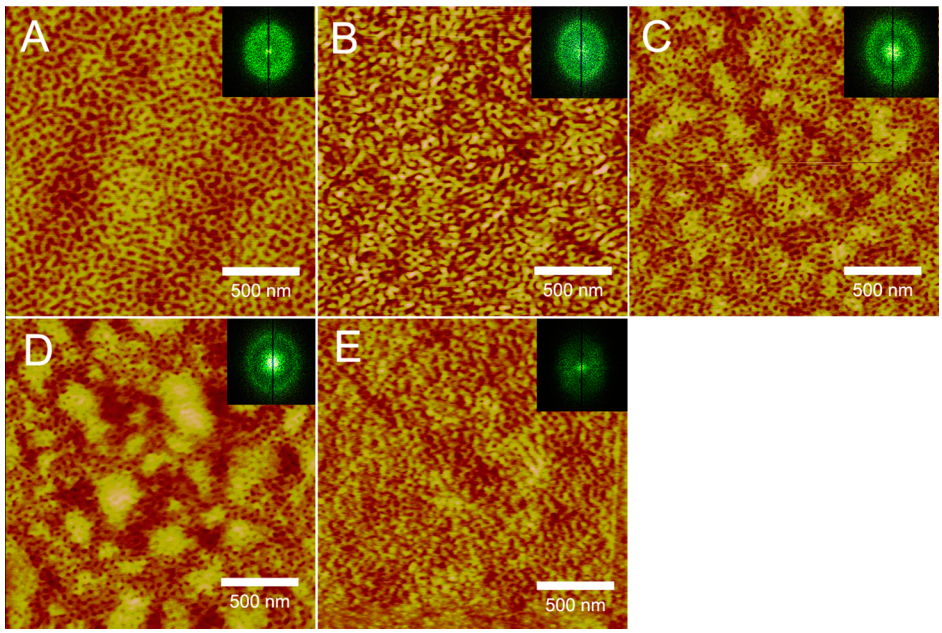

Figure 1. AFM micrographs (height image) of BuNB-*b*-HFANB films after SVA using (A) toluene, (B) THF, (C) dioxane, and (D) DMF as well as the (E) as-cast film. FFTs of the images are shown in the insets.

DOI: 10.1021/acsami.5b02692
ACS Appl. Mater. Interfaces 2015, 7, 11765−11774

this series.[47] For SVA using THF (Figure 1B), the surface morphology is only slightly altered, but it is better resolved by AFM; there is still a lack of long-range order and the associated space group for the surface morphology is difficult to ascertain. There are two possible explanations for this behavior: First, there is insufficient solvent in the film to plasticize the BCP to enable segmental rearrangements necessary to enable long-range ordering. Second, as THF is only a modest hydrogen bond acceptor, the physical cross-links associated with the hydrogen bonding of the HFANB domains cannot be displaced easily by THF to enable ordering. Using dioxane as the solvent for SVA yields a marked change in the surface morphology with an increase in the uniformity of the nanostructure with a predominance of the circular surface structure (Figure 1C); we attribute these surface structures to vertically aligned cylinders (as will be confirmed later from GISAXS measurements). As BuNB-*b*-HFANB swells nominally the same in dioxane and THF, the hydrogen bond acceptor strength of the solvent used in SVA appears to be a critical component to the efficacy in obtaining a well-ordered morphology in BuNB-*b*-HFANB, although solvent selectivity during SVA is known to be important to generate long-range ordering.[28,48] The strength of the hydrogen bonding acceptor increases with the use of DMF (Figure 1D) and the ordering appears to improve with primarily perpendicular orientation of the cylindrical domains. It is difficult to assess, however, if these circular surface structures are indeed perpendicular cylinders from the AFM measurements alone.

To understand better the morphology of these films, GISAXS has been employed to elucidate further information about their self-assembled structure. As shown in Figure 2, the GISAXS patterns are impacted by selection of SVA solvent. In all cases, one order of diffraction associated with the in-plane film correlations is clearly observed; the lack of higher order reflections is consistent with the lack of long-range order

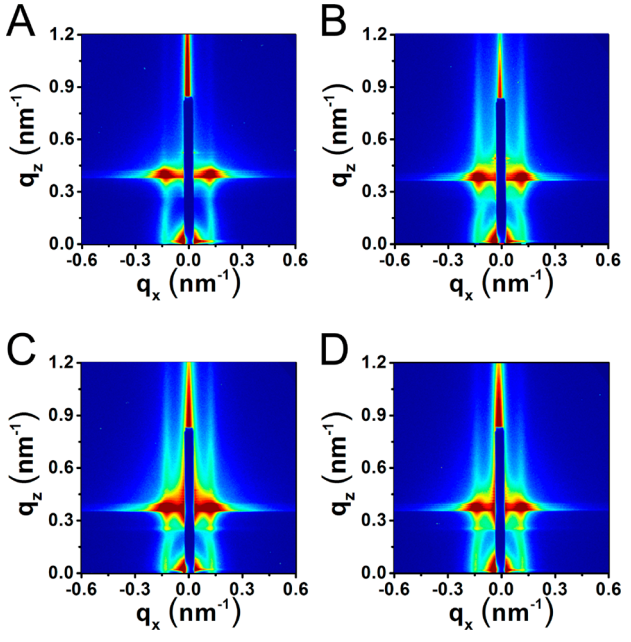

Figure 2. GISAXS profiles associated with SVA using (A) toluene, (B) THF, (C) dioxane, and (D) DMF for BuNB-*b*-HFANB films. The incident angle is 0.2°, which is greater than the critical angle to probe the entire thickness of the film.

observed in the AFM micrographs. The *d*-spacing associated with the primary diffraction peak is invariant for all SVA conditions utilized (48.5 ± 1.6 nm) and is consistent with the *d*-spacing obtained from the weak diffraction of the as-cast film (Figure S7 of the Supporting Information); this consistency in *d*-spacing is further evidence that the cylindrical morphology is not likely a kinetically trapped state. Further examination of the GISAXS profiles yields insight into the morphology. For the SVA with toluene (Figure 2A), a weak streak in q_z emanating from the primary diffraction peak is present along with a weak diffraction spot behind the beamstop at approximately $q_z = 0.05$ Å^{-1}. These components to the GISAXS pattern suggest both vertical (streaks) and parallel (diffraction spot behind beamstop) components to the structure (coexistence). Note that isotropic cylinders in three dimensions would yield a ring pattern, so there is a clear preference even when weakly ordered for BuNB-*b*-HFANB domains to orient relative to the interfaces. This weak scattering in Figure 2A suggesting coexistence of parallel and perpendicular structures is consistent with the weakly ordered surface morphology determined from AFM, where short rod-like structure and spots can be resolved in the micrographs. For SVA using THF (Figure 2B), both of these features are still present. However, the ordering using THF is improved as evidenced by the increased scattered intensity (same acquisition time and film thickness) with both the streak and diffraction spot behind the beamstop in the GISAXS pattern more clearly resolved. This compares well with the surface morphology determined by AFM where the nanostructure (Figure 1B) is more clearly resolved than after SVA with toluene (Figure 1A), but there is no clear change in the overall structure. With the use of dioxane (Figure 2C), the streaks in the GISAXS profile are better resolved, but diffraction spot behind the beamstop is not as clearly defined; this suggests a decrease in parallel alignment with SVA using dioxane such that a majority of the cylinders are perpendicularly oriented. This is consistent with the AFM micrograph in Figure 1C where the surface contains primarily circular patterns that can be attributed to the ends of cylinders. In Figure 2D, the diffraction spot behind the beamstop is no longer clearly observable, which suggests that the ordered system is primarily vertically oriented cylinders with SVA using DMF. These GISAXS patterns (Figure 2) are, in general, consistent with the surface morphology elucidated from AFM (Figure 1). Both AFM and GISAXS suggest that the density of vertically oriented cylinders increases as the solubility parameter and hydrogen bond acceptor strength of the solvent used in SVA increase. Interestingly, there appears to be propensity for the perpendicular orientation of the cylindrical nanostructure in these films. This behavior is unusual as typically the SVA solvent must produce a neutral wetting surface to promote perpendicular orientation.[48] Although the morphology of the films evolves during SVA, ordering of the self-assembled structure is highly limited. Even for the film after SVA with DMF, which exhibits primarily perpendicular orientation of the cylinders, the expected hexagonal packing cannot be discerned, even locally from AFM (Figure 1D). This limited long-range order is not necessarily a limitation for BCPs in membranes. The preferential vertical orientation could provide the requisite transport pathways to tremendously impact the performance. Previously, Balsara and co-workers have illustrated that poorly ordered BCPs can exhibit high performance as Li ion electrolytes where transport of Li^+ and mechanical properties are important.[49] One challenge for

DOI: 10.1021/acsami.5b02692
ACS Appl. Mater. Interfaces 2015, 7, 11765−11774

commercialization of poorly ordered BCPs is how to assess reproducibility of the nanostructure if slight variations impact the performance. We hypothesize that the mechanical properties from wrinkling may provide one such route.

For membrane commercialization, the mechanical properties are critical to its ultimate utility as insufficient mechanical integrity can lead to premature failure. Simple measurement of the bulk mechanical properties of BCPs proposed for use in membranes may not provide an accurate assessment of these properties in an active membrane. First, the extent of orientation/alignment of BCPs can significantly impact the measured mechanical properties.[3,50] Second, the properties of thin films can differ from the bulk;[51] the aging characteristics of membranes can be significantly altered even for micrometer thicknesses.[52] To assess directly the modulus of the BCP films, surface wrinkling is employed for the different SVA treatments. Figure 3 illustrates that the elastic modulus for the neat BuNB-*b*-HFANB films is enhanced with the use of the more polar solvents in SVA, which leads to a more ordered morphology. Without SVA, the film is poorly ordered with an average elastic modulus of 1.44 GPa. Exposure to toluene vapor only slightly increases the ordering and the average elastic modulus increases to 1.56 GPa. The intrinsic scatter with mechanical measurements leads to uncertainty in the statistical differences between these two samples, but further improvement in the ordering by use of THF SVA leads to statistically significant difference with the as-cast film. Interestingly, there appears to be a limit in the enhancement in the elastic modulus for these films as SVA with THF, dioxane, or DMF produces moduli that are statistically identical, despite the further improvement in order with the increasing polarity of the solvent. This strong dependence of elastic modulus on weak ordering of BCPs has not been reported previously for bulk systems, but processing into coupons for mechanical testing tends to order and align the BCPs. The perpendicular oriented cylindrical domains in BCP thin film should lead to anisotropic mechanical properties in plane and out of plane of the film. The elastic modulus parallel to the domains orientation direction usually significantly increases especially for two domains having very different mechanical properties.[53,54] However, the elastic modulus perpendicular to the domains orientation direction shows invariant,[50,55] decreased[56] or increased modulus[54] compared to the corresponding isotropic materials for BCP and aligned semicrystalline polymers based on prior reports. As the elastic modulus measured by surface wrinkling depends on a compressive stress in plane of the film, the measurement probes the compressive modulus parallel to the film plane, which is the direction perpendicular to the cylindrical domains orientation direction. Thus, the increased modulus of BuNB-*b*-HFANB films using SVA may be partially ascribed to this orientation effect. On the other hand, the change in orientation and ordering of the block copolymers will impact the chain stretching.[57,58] For the copolymer system of Nafion, confinement dramatically increases the stiffness, which is attributed to individual chain properties due to chain extension.[59] Thus, the results here are also consistent with this chain stretching argument.

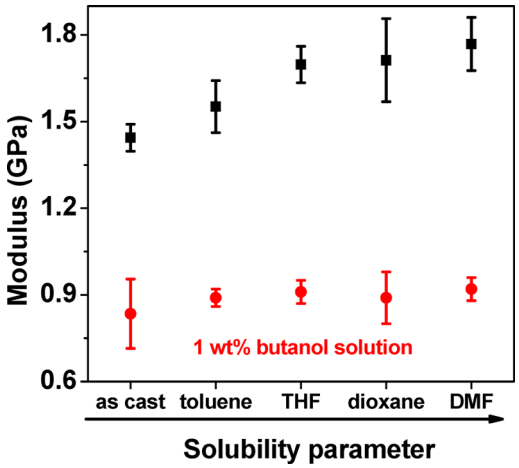

Figure 3. Elastic modulus of BuNB-*b*-HFANB films as a function of solvent used from SVA for the (■) neat film and (●) after being swollen by exposure to 1 wt % butanol solution.

To elucidate comprehensively the morphology effect on the mechanical properties, the fracture strength and onset fracture strain of BuNB-*b*-HFANB thin films treated with SVA using different solvents were characterized using cracking measurement. In the linear regime of thin film cracking on a compliant substrate, the average crack spacing is inversely proportional to the applied stretching strain,[30] that is

$$\langle d \rangle = \frac{2h_f\sigma^*}{E_s(\varepsilon - \varepsilon^*)} \quad (1)$$

where $\langle d \rangle$ is the average crack spacing, h_f is the film thickness, E_s is the Young's modulus of substrate, ε is the applied stretching strain, ε^* is the onset fracture strain, and σ^* is the fracture strength.

Figure S9 of the Supporting Information shows the typical crack propagation of BuNB-*b*-HFANB thin films supported on PDMS substrate. The thin films start to show a few parallel cracks perpendicular to the stretching direction when the strain is 1%. Because the films are brittle rather than ductile, the cracks appear first whereas wrinkling occurs at higher strains. As the strain increases in steps of 0.3%, new cracks continuously propagate, resulting in a reduced cracking spacing. Because the stretching strain for BuNB-*b*-HFANB thin films is small (<3.5%) in all cases, the PDMS substrate is known to show linear elastic behavior at this region. Thus, eq 1 can be applied to describe the relation between the fracture strength and onset fracture strain. Figure 4 shows the plot of eq 1 for 145 nm BuNB-*b*-HFANB thin film (SVA using DMF). The crack density ($1/\langle d \rangle$) increases linearly with increasing strain, which

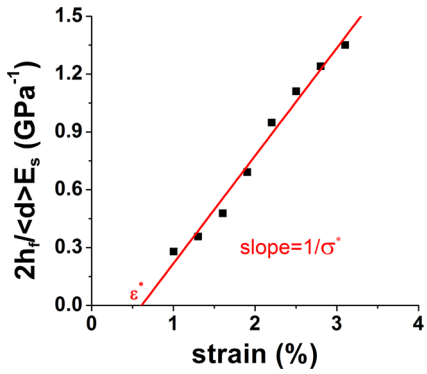

Figure 4. Determination of fracture properties of 145 nm BuNB-*b*-HFANB thin film (SVA using DMF) as determined from quantification of the crack density as a function of strain.

DOI: 10.1021/acsami.5b02692
ACS Appl. Mater. Interfaces 2015, 7, 11765−11774

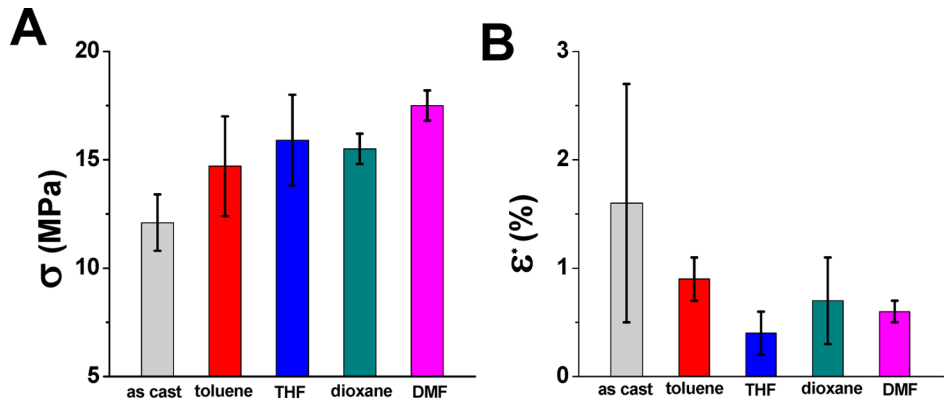

Figure 5. (A) Fracture strength and (B) onset fracture strain of BuNB-*b*-HFANB films as a function of solvent used for SVA.

is consistent with eq 1 for describing the cracking behavior of the thin films in this region. The linear fit yields the fracture strength and onset fracture strain of the thin films from the slope and the *x*-intercept, respectively.

Figure 5 illustrates how the fracture strength and onset fracture strain of films depends on the solvent selection for SVA. Similar to the enhancement of modulus as the ordering of structure in thin films was improved, the fracture strength of thin films increases from 12.1 to 17.5 MPa going from the as-cast film to the one ordered using DMF for the SVA process. Although the fracture strength after SVA is significantly improved compared to the as-cast films, the onset fracture strain decreases from 1.6% to approximately 0.7%. These results suggest that the mechanical properties of thin films are very sensitive to minor changes in their ordering.

For membrane separation of biobutanol from a fermentation broth,[60] the solubility of butanol in the BuNB-*b*-HFANB is important if the separation is driven by solution-diffusion as is common for polymer membranes.[61] To assess the absorption of butanol in the films, the mass uptake from aqueous butanol solutions is assessed using QCM-D. Unfortunately, the time associated with the changing the QCM-D cell from water to butanol (as assessed by a blank crystal) is nearly indistinguishable to the time associated with swelling of the BuNB-*b*-HFANB films (see the Supporting Information). Thus, only equilibrium absorption capacities are reported. Figure 6 illustrates the sorption isotherm associated with changes in the butanol concentration from 0 to 5 wt % in aqueous solution. For pure water, water absorbed by films is estimated to be approximately 1.3% on the basis of the actual and expected frequency shift associated with the kinematic viscosity of water.[41] The surface of BuNB-*b*-HFANB films is slightly rougher than the bare quartz sensor, so some of the frequency change can be attributed to the roughness of film. As might be expected, the absorption capacity is nearly invariant of the processing. Interestingly, there appears to be a slight decrease in uptake for the most highly ordered film using DMF as the SVA solvent. From a simplistic view, the solubility should be independent of ordering as the global composition is invariant. The ordering that leads to some stretching at the interface[62] could enhance the solubility. This is clearly not the case here, as the most ordered sample appears to have the least uptake of butanol. With the perpendicular orientation, the swelling of the domains may be more constrained as the film is confined to the substrate and only expansion perpendicular to the substrate is available; thus, the BuNB domains act as physical cross-links, which in the perpendicular orientation are fixed by the substrate. This hypothesis is consistent with increase in the deviation of the film that is SVA with DMF compared to the other films as the uptake is increased. In all cases, the uptake increases linearly with increasing concentration of butanol in the aqueous solution. As low concentrations are examined, this linear uptake can be quantified through Henry's law. The Henry's law constant is 5.0 from the linear fit of the concentration for bulk solutions of ≤1 wt % butanol. From the solution diffusion mechanism, the solubility and relative concentration of butanol in the BCP are directly related to the permeance and the selectivity of the membrane. Typical titers for biobutanol are approximately 1−2%, which would suggest a solubility of 5.0−10.0 wt % in the membrane. One challenge is to understand the butanol−water selectivity, as it is difficult to quantify spectroscopically the concentrations, as the hydroxyl in water is also present in the HFANB segments and butanol, as well as the alkyl chain in butanol, is also present in the BuNB segments. This significantly limits the sensitivity to determine the selectivity of the membrane from sorption measurements. Nonetheless, these measurements provide insight into the total solvent content in the membrane under operating conditions, which can be utilized to determine how other physical properties of the membrane may be affected.

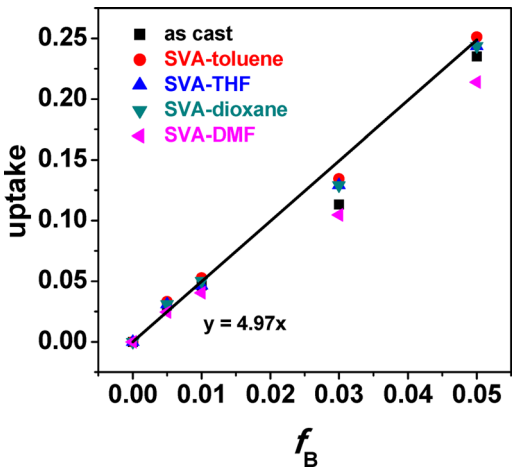

Figure 6. Swelling of BuNB-*b*-HFANB films by aqueous butanol solutions as determined by QCM-D. The uptake is the weight fraction change relative to the equilibrated film in pure water.

By examining the BuNB-*b*-HFANB films under conditions that mimic operation, a different conclusion is drawn regarding the effect of SVA processing on the mechanical properties. As

DOI: 10.1021/acsami.5b02692
ACS Appl. Mater. Interfaces 2015, 7, 11765−11774

shown in Figure 3, there is no difference in the elastic modulus of these films after immersion in 1 wt % aqueous butanol. In all cases, the films contain only approximately 5.0 wt % butanol/water and are greatly plasticized, as evidenced by the decrease in modulus to approximately 0.9 GPa. This is at least a 38% decrease in the modulus in comparison to the dry BCP film. Compared to other plasticized films, this decrease in modulus is very large. For example, the modulus of polystyrene containing 5 wt % of DOP is nearly unchanged with respect to the modulus of the neat polystyrene.[31] The reason for the large decrease in modulus is that the solvent is not homogeneously distributed in the BCP film, which then significantly swells only one phase (HFANB in this case). To prove this, the swelling and elastic modulus of both the BuNB and HFANB homopolymers were investigated by ellipsometry and surface wrinkling, respectively. When the BuNB homopolymer thin films are immersed in 1 wt % aqueous butanol, the thickness does not change statistically and the modulus is invariant at 1.1 GPa. In contrast, the thickness of HFANB homopolymer thin films increases by 9.9% in 1 wt % aqueous butanol and, correspondingly, the modulus significantly decreases from 1.80 to 0.43 GPa. This swelling of the homopolymers is consistent with the volume fraction averaged swelling of the BCP.

As the elastic modulus of dry films and swollen films in 1 wt % aqueous butanol differ substantially, as discussed previously, it is not surprising that the cracking behavior of swollen films is also significantly impacted by the sorption of aqueous butanol. The dry BuNB-*b*-HFANB films are very brittle with the onset fracture strain of 0.4−1.6%, whereas the films swollen by approximately 5.0 wt % butanol were quite ductile with the onset fracture strain extended to 6−7%, as shown in Figure 7c. These swollen films show fewer cracks and these cracks are small and do not appear to propagate significantly even at high strain (20%). This behavior is quite different from the dry films, which show a much higher crack density and propagation at modest strain (6.5%), as shown in Figure 7. The improved ductility of the BCP under simulated operating conditions would likely be beneficial to inhibit cracks and other catastrophic failures of the membrane.

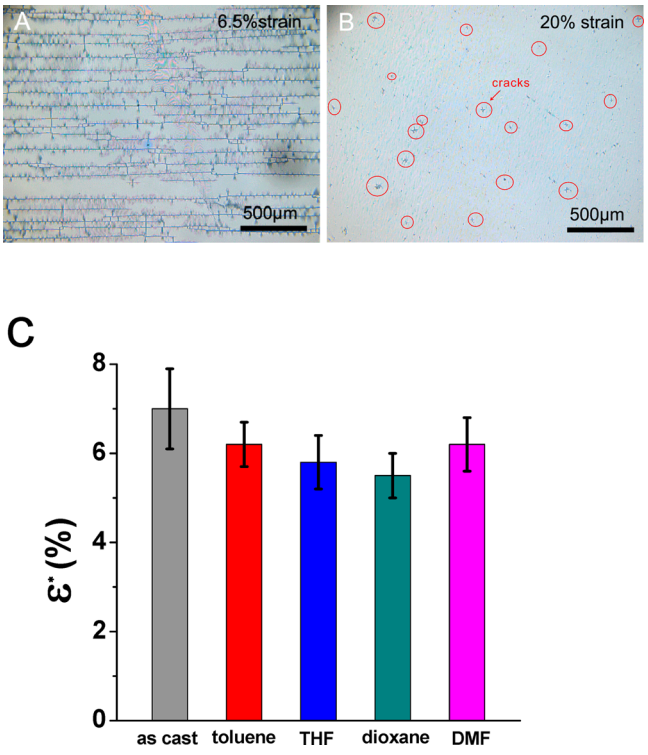

Figure 7. Crack patterns of 140 nm BuNB-*b*-HFANB thin films at (A) 6.5% strain for neat film and (B) 20% strain when swollen with approximately 5.0 wt % butanol. (C) Onset fracture strain of BuNB-*b*-HFANB films (SVA using different solvents) swollen with approximately 5.0 wt % butanol.

CONCLUSIONS

The morphology of BuNB-*b*-HFANB films with segmental T_g's exceeding 300 °C was tuned by solvent selection for SVA. The SVA solvent selection can modestly adjust the extent of perpendicularly oriented cylinders in the ordered nanostructure, but these perpendicular cylinders persist over a wide range of solubility parameters when the films can be ordered. The elastic modulus and fracture strength of BuNB-*b*-HFANB films were enhanced when the extent of ordering was increased. The elastic modulus increases to 1.77 GPa when the films were SVA using DMF, whereas the films without SVA processing exhibit a lower modulus of 1.44 GPa. Additionally, the fracture strength of the films with improved ordering increases from 12.1 to 17.5 MPa, whereas the onset fracture strain decreases from 1.6% to approximately 0.6%. These results indicate that minor changes in the ordered structure of BCP thin films can appreciably impact the mechanical properties, even when both phases are glassy. From 1 wt % butanol solution, the BuNB-*b*-HFANB films are swollen with approximately 5 wt % of butanol. This sorption decreases the elastic modulus significantly to approximately 0.89 GPa; this swollen modulus is independent of the nanostructure despite the significant differences in the dry state. Interestingly, the toughness of the BuNB-*b*-HFANB films appears to increase appreciably by swelling with small fractions of butanol as the onset fracture strain increases by almost 1 order of magnitude and the crack propagation is nearly arrested even at high strain.

ASSOCIATED CONTENT

Supporting Information

GPC traces and ^{13}C NMR for the BCP; calculation of Hansen solubility parameters for BuNB and HFANB homopolymers using group contribution method; solvent swelling dynamics for BuNB and HFANB homopolymers; AFM images of the as-cast and thermally annealed film; cross-sectional TEM of BuNB/HFANB homopolymer bilayer and TEM image of BuNB-*b*-HFANB thin film; GISAXS of the as-cast film; diffusion dynamics of butanol for BuNB-*b*-HFANB films studied using QCM-D; optical micrographs of the cracked films and AFM micrograph of BuNB-*b*-HFANB film after swollen in 1 wt % aqueous butanol. The Supporting Information is available free of charge on the ACS Publications website at DOI: 10.1021/acsami.5b02692.

AUTHOR INFORMATION

Corresponding Author

*B. D. Vogt. E-mail: vogt@uakron.edu.

Author Contributions

The paper was written through contributions of all authors. All authors have given approval to the final version of the paper.

Notes

The authors declare no competing financial interest.

DOI: 10.1021/acsami.5b02692
ACS Appl. Mater. Interfaces 2015, 7, 11765−11774

■ ACKNOWLEDGMENTS

Use of the National Synchrotron Light Source, Brookhaven National Laboratory, was supported by the U.S. Department of Energy, Office of Science, Office of Basic Energy Sciences, under Contract No. DE-AC02-98CH10886. Portions of this work were performed at the Center for Functional Nanomaterials, Brookhaven National Laboratory, which is supported by the U.S. Department of Energy, Office of Basic Energy Sciences, under Contract No. DE-AC02-98CH10886. We thank Prasad Raut and Prof. Sadhan Jana for assistance with the density determination using the helium pychnometer. We also thank Clinton Wiener, Jeongwoo Lee and Bo Ni for their assistance with QCM and TEM measurements.

■ REFERENCES

(1) Bates, F. S.; Hillmyer, M. A.; Lodge, T. P.; Bates, C. M.; Delaney, K. T.; Fredrickson, G. H. Multiblock Polymers: Panacea or Pandora's Box? *Science* **2012**, *336*, 434−440.

(2) Spontak, R. J.; Patel, N. P. Thermoplastic Elastomers: Fundamentals and Applications. *Curr. Opin. Colloid Interface Sci.* **2000**, *5*, 334−341.

(3) Honeker, C. C.; Thomas, E. L. Impact of Morphological Orientation in Determining Mechanical Properties in Triblock Copolymer Systems. *Chem. Mater.* **1996**, *8*, 1702−1714.

(4) Sun, F. M.; Ruckenstein, E. Membranes of Block-Copolymer Poly(divinylbenzene) Blends for the Pervaporation of Alcohol-Water Mixtures. *J. Membr. Sci.* **1994**, *90*, 275−282.

(5) Miyata, T.; Obata, S.; Uragami, T. Morphological Effects of Microphase Separation on the Permselectivity for Aqueous Ethanol Solutions of Block and Graft Copolymer Membranes Containing Poly(dimethylsiloxane). *Macromolecules* **1999**, *32*, 3712−3720.

(6) Jha, A. K.; Tsang, S. L.; Ozcam, A. E.; Offeman, R. D.; Balsara, N. P. Master Curve Captures the Effect of Domain Morphology on Ethanol Pervaporation through Block Copolymer Membranes. *J. Membr. Sci.* **2012**, *401*−*402*, 125−131.

(7) Ulbricht, M. Advanced Functional Polymer Membranes. *Polymer* **2006**, *47*, 2217−2262.

(8) Huang, H.-J.; Ramaswamy, S.; Tschirner, U. W.; Ramarao, B. V. A Review of Separation Technologies in Current and Future Biorefineries. *Sep. Purif. Technol.* **2008**, *62*, 1−21.

(9) Crowhurst, N. A.; Leak, D. J. Biobutanol: A Better Biofuel? *Int. Sugar J.* **2010**, *112*, 64−73.

(10) Kaminski, W.; Tomczak, E.; Gorak, A. Biobutanol - Production and Purification Methods. *Ecol. Chem. Eng. S* **2011**, *18*, 31−37.

(11) Geise, G. M.; Freeman, B. D.; Paul, D. R. Characterization of a Sulfonated Pentablock Copolymer for Desalination Applications. *Polymer* **2010**, *51*, 5815−5822.

(12) Fasolka, M. J.; Mayes, A. M. Block Copolymer Thin Films: Physics and Applications. *Annu. Rev. Mater. Res.* **2001**, *31*, 323−355.

(13) Morkved, T. L.; Lu, M.; Urbas, A. M.; Ehrichs, E. E.; Jaeger, H. M.; Mansky, P.; Russell, T. P. Local Control of Microdomain Orientation in Diblock Copolymer Thin Films with Electric Fields. *Science* **1996**, *273*, 931−933.

(14) Park, M.; Harrison, C.; Chaikin, P. M.; Register, R. A.; Adamson, D. H. Block Copolymer Lithography: Periodic Arrays of Similar to 10(11) Holes in 1 Square Centimeter. *Science* **1997**, *276*, 1401−1404.

(15) Ruiz, R.; Kang, H.; Detcheverry, F. A.; Dobisz, E.; Kercher, D. S.; Albrecht, T. R.; de Pablo, J. J.; Nealey, P. F. Density Multiplication and Improved Lithography by Directed Block Copolymer Assembly. *Science* **2008**, *321*, 936−939.

(16) Ryu, D. Y.; Shin, K.; Drockenmuller, E.; Hawker, C. J.; Russell, T. P. A Generalized Approach to The Modification of Solid Surfaces. *Science* **2005**, *308*, 236−239.

(17) Kim, S. O.; Solak, H. H.; Stoykovich, M. P.; Ferrier, N. J.; de Pablo, J. J.; Nealey, P. F. Epitaxial Self-Assembly of Block Copolymers on Lithographically Defined Nanopatterned Substrates. *Nature* **2003**, *424*, 411−414.

(18) Bates, C. M.; Seshimo, T.; Maher, M. J.; Durand, W. J.; Cushen, J. D.; Dean, L. M.; Blachut, G.; Ellison, C. J.; Willson, C. G. Polarity-Switching Top Coats Enable Orientation of Sub-10-nm Block Copolymer Domains. *Science* **2012**, *338*, 775−779.

(19) Seshimo, T.; Bates, C. M.; Dean, L. M.; Cushen, J. D.; Durand, W. J.; Maher, M. J.; Ellison, C. J.; Willson, C. G. Block Copolymer Orientation Control Using a Top-Coat Surface Treatment. *J. Photopolymer Sci. Technol.* **2012**, *25*, 125−129.

(20) Thurn-Albrecht, T.; DeRouchey, J.; Russell, T. P.; Kolb, R. Pathways toward Electric Field Induced Alignment of Block Copolymers. *Macromolecules* **2002**, *35*, 8106−8110.

(21) Liedel, C.; Pester, C. W.; Ruppel, M.; Lewin, C.; Pavan, M. J.; Urban, V. S.; Shenhar, R.; Boesecke, P.; Boeker, A. Block Copolymer Nanocomposites in Electric Fields: Kinetics of Alignment. *ACS Macro Lett.* **2013**, *2*, 53−58.

(22) Singh, G.; Yager, K. G.; Smilgies, D.-M.; Kulkarni, M. M.; Bucknall, D. G.; Karim, A. Tuning Molecular Relaxation for Vertical Orientation in Cylindrical Block Copolymer Films via Sharp Dynamic Zone Annealing. *Macromolecules* **2012**, *45*, 7107−7117.

(23) Lin, Z. Q.; Kim, D. H.; Wu, X. D.; Boosahda, L.; Stone, D.; LaRose, L.; Russell, T. P. A Rapid Route to Arrays of Nanostructures in Thin Films. *Adv. Mater.* **2002**, *14*, 1373−1376.

(24) Fukunaga, K.; Elbs, H.; Magerle, R.; Krausch, G. Large-Scale Alignment of ABC Block Copolymer Microdomains via Solvent Vapor Treatment. *Macromolecules* **2000**, *33*, 947−953.

(25) Kim, S. H.; Misner, M. J.; Xu, T.; Kimura, M.; Russell, T. P. Highly Oriented and Ordered Arrays from Block Copolymers via Solvent Evaporation. *Adv. Mater.* **2004**, *16*, 226.

(26) Jung, Y. S.; Ross, C. A. Solvent-Vapor-Induced Tunability of Self-Assembled Block Copolymer Patterns. *Adv. Mater.* **2009**, *21*, 2540−2545.

(27) Albert, J. N. L.; Bogart, T. D.; Lewis, R. L.; Beers, K. L.; Fasolka, M. J.; Hutchison, J. B.; Vogt, B. D.; Epps, T. H. Gradient Solvent Vapor Annealing of Block Copolymer Thin Films Using a Microfluidic Mixing Device. *Nano Lett.* **2011**, *11*, 1351−1357.

(28) Gotrik, K. W.; Hannon, A. F.; Son, J. G.; Keller, B.; Alexander-Katz, A.; Ross, C. A. Morphology Control in Block Copolymer Films Using Mixed Solvent Vapors. *ACS Nano* **2012**, *6*, 8052−8059.

(29) Kusoglu, A.; Santare, M. H.; Karlsson, A. M. Aspects of Fatigue Failure Mechanisms in Polymer Fuel Cell Membranes. *J. Polym. Sci., Part B: Polym. Phys.* **2011**, *49*, 1506−1517.

(30) Chung, J. Y.; Lee, J.-H.; Beers, K. L.; Stafford, C. M. Stiffness, Strength, and Ductility of Nanoscale Thin Films and Membranes: A Combined Wrinkling-Cracking Methodology. *Nano Lett.* **2011**, *11*, 3361−3365.

(31) Stafford, C. M.; Harrison, C.; Beers, K. L.; Karim, A.; Amis, E. J.; Vanlandingham, M. R.; Kim, H. C.; Volksen, W.; Miller, R. D.; Simonyi, E. E. A Buckling-based Metrology for Measuring the Elastic Moduli of Polymeric Thin Films. *Nat. Mater.* **2004**, *3*, 545−550.

(32) Dair, B. J.; Honeker, C. C.; Alward, D. B.; Avgeropoulos, A.; Hadjichristidis, N.; Fetters, L. J.; Capel, M.; Thomas, E. L. Mechanical Properties and Deformation Behavior of the Double Gyroid Phase in Unoriented Thermoplastic Elastomers. *Macromolecules* **1999**, *32*, 8145−8152.

(33) Cohen, Y.; Albalak, R. J.; Dair, B. J.; Capel, M. S.; Thomas, E. L. Deformation of Oriented Lamellar Block Copolymer Films. *Macromolecules* **2000**, *33*, 6502−6516.

(34) Ryu, C. Y.; Ruokolainen, J.; Fredrickson, G. H.; Kramer, E. J.; Hahn, S. F. Chain Architecture Effects on Deformation and Fracture of Block Copolymers with Unentangled Matrices. *Macromolecules* **2002**, *35*, 2157−2166.

(35) Lee, J. Y.; Crosby, A. J. Crazing in Glassy Block Copolymer Thin Films. *Macromolecules* **2005**, *38*, 9711−9717.

(36) Croll, A. B.; Crosby, A. J. Pattern Driven Stress Localization in Thin Diblock Copolymer Films. *Macromolecules* **2012**, *45*, 4001−4006.

(37) Bedwell, B.; Elce, E.; Knapp, B.; Langsdorf, L. J.; Wilks, R.; Naep, B.; Elseu, E.; Rangseudopeu, R. J.; Wilkeuseu, R.; Wilkes, R.

DOI: 10.1021/acsami.5b02692
ACS Appl. Mater. Interfaces 2015, 7, 11765−11774

Pervaporation Membrane, Useful for Separating Organic Product (Butanol) from Fermentation Broth, and Organic Material from Water, Comprises Vinyl Addition Polynorbornene Polymer Having Specific Molecular Weight and Separation Factor. US2009188863-A1; WO2009097322-A1; TW200946216-A; EP2238179-A1; KR2010119778-A; CN101970509-A; JP2011510805-W; US8215496-B2.

(38) Dorkenoo, K. D.; Pfromm, P. H.; Rezac, M. E. Gas Transport Properties of a Series of High T_g Polynorbornenes with Aliphatic Pendant Groups. *J. Polym. Sci., Part B: Polym. Phys.* **1998**, *36*, 797−803.

(39) Qiang, Z.; Zhang, L. H.; Stein, G. E.; Cavicchi, K. A.; Vogt, B. A. Unidirectional Alignment of Block Copolymer Films Induced by Expansion of a Permeable Elastomer during Solvent Vapor Annealing. *Macromolecules* **2014**, *47*, 1109−1116.

(40) Rodahl, M.; Hook, F.; Krozer, A.; Brzezinski, P.; Kasemo, B. Quartz-Crystal Microbalance Setup for Frequency and Q-Factor Measurements in Gaseous and Liquid Environments. *Rev. Sci. Instrum.* **1995**, *66*, 3924−3930.

(41) Cho, N.-J.; D'Amour, J. N.; Stalgren, J.; Knoll, W.; Kanazawa, K.; Frank, C. W. Quartz Resonator Signatures Under Newtonian Liquid Loading For Initial Instrument Check. *J. Colloid Interface Sci.* **2007**, *315*, 248−254.

(42) Sauerbrey, G. Z. Verwendung von Schwingquarzen zur Wagung dunner Schichten und zur Mikrowagung. *Z. Phys.* **1959**, *155*, 206−222.

(43) Stafford, C. M.; Guo, S.; Harrison, C.; Chiang, M. Y. M. Combinatorial and High-Throughput Measurements of the Modulus of Thin Polymer Films. *Rev. Sci. Instrum.* **2005**, *76*, 062207.

(44) Paik, M. Y.; Bosworth, J. K.; Smilges, D. M.; Schwartz, E. L.; Andre, X.; Ober, C. K. Reversible Morphology Control in Block Copolymer Films via Solvent Vapor Processing: An in Situ GISAXS Study. *Macromolecules* **2010**, *43*, 4253−4260.

(45) Hansen, C. M. *Hensen Solubility Parameters, A User's Handbook*; CRC Press: Boca Raton, FL, 2000.

(46) Funaki, Y.; Kumano, K.; Nakao, T.; Jinnai, H.; Yoshida, H.; Kimishima, K.; Tsutsumi, K.; Hirokawa, Y.; Hashimoto, T. Influence of Casting Solvents on Microphase-Separated Structures of Poly(2-vinylpyridine)-Block-Polyisoprene. *Polymer* **1999**, *40*, 7147−7156.

(47) Abraham, M. H. Scales Of Solute Hydrogen-Bonding - Their Construction and Application to Physicochemical and Biochemical Processes. *Chem. Soc. Rev.* **1993**, *22*, 73−83.

(48) Sinturel, C.; Vayer, M.; Morris, M.; Hillmyer, M. A. Solvent Vapor Annealing of Block Polymer Thin Films. *Macromolecules* **2013**, *46*, 5399−5415.

(49) Singh, M.; Odusanya, O.; Wilmes, G. M.; Eitouni, H. B.; Gomez, E. D.; Patel, A. J.; Chen, V. L.; Park, M. J.; Fragouli, P.; Iatrou, H.; Hadjichristidis, N.; Cookson, D.; Balsara, N. P. Effect of Molecular Weight on the Mechanical and Electrical Properties of Block Copolymer Electrolytes. *Macromolecules* **2007**, *40*, 4578−4585.

(50) Ye, C. H.; Singh, G.; Wadley, M. L.; Karim, A.; Cavicchi, K. A.; Vogt, B. D. Anisotropic Mechanical Properties of Aligned Polystyrene-Block-Polydimethylsiloxane Thin Films. *Macromolecules* **2013**, *46*, 8608−8615.

(51) Stafford, C. M.; Vogt, B. D.; Harrison, C.; Julthongpiput, D.; Huang, R. Elastic Moduli of Ultrathin Amorphous Polymer Films. *Macromolecules* **2006**, *39*, 5095−5099.

(52) Xia, J.; Chung, T.-S.; Li, P.; Horn, N. R.; Paul, D. R. Aging and Carbon Dioxide Plasticization of Thin Polyetherimide Films. *Polymer* **2012**, *53*, 2099−2108.

(53) Arridge, R. G. C.; Folkes, M. J. The Mechanical Properties of a "Single Crystal" of SBS Copolymer - A Novel Composite Material. *J. Phys. Part D: Appl. Phys.* **1972**, *5*, 344−358.

(54) Raumann, G.; Saunders, D. W. The Anisotropy of Young's Modulus in Drawn Polyethylene. *Proc. Phys. Soc.* **1961**, *77*, 1028−1037.

(55) Razavi-Nouri, M.; Hay, J. N. Effect Of Orientation On Mechanical Properties Of Metallocene Polyethylenes. *Iranian Polym. J.* **2004**, *13*, 521−530.

(56) Gupta, V. B.; Ward, I. M. Mechanical and Optical Anisotropy in Low-Density Polyethylene. *J. Macromol. Sci., Phys.* **1967**, *1*, 373−400.

(57) Wu, L. F.; Lodge, T. P.; Bates, F. S. Effect of Block Number on Multiblock Copolymer Lamellae Alignment under Oscillatory Shear. *J. Rheol.* **2005**, *49*, 1231−1252.

(58) Schmidt, K.; Schoberth, H. G.; Ruppel, M.; Zettl, H.; Hansel, H.; Weiss, T. M.; Urban, V.; Krausch, G.; Boker, A. Reversible Tuning of a Block-Copolymer Nanostructure via Electric Fields. *Nat. Mater.* **2008**, *7*, 142−145.

(59) Page, K. A.; Kusoglu, A.; Stafford, C. M.; Kim, S.; Kline, R. J.; Weber, A. Z. Confinement-Driven Increase in Ionomer Thin-Film Modulus. *Nano Lett.* **2014**, *14*, 2299−2304.

(60) Garcia, V.; Pakkila, J.; Ojamo, H.; Muurinen, E.; Keiski, R. L. Challenges in Biobutanol Production: How to Improve the Efficiency? *Renewable Sustainable Energy Rev.* **2011**, *15*, 964−980.

(61) Abdehagh, N.; Tezel, F. H.; Thibault, J. Separation Techniques in Butanol Production: Challenges and Developments. *Biomass Bioenergy* **2014**, *60*, 222−246.

(62) Matsen, M. W.; Bates, F. S. Block Copolymer Microstructures in the Intermediate-Segregation Regime. *J. Chem. Phys.* **1997**, *106*, 2436−2448.

DOI: 10.1021/acsami.5b02692
ACS Appl. Mater. Interfaces 2015, 7, 11765−11774